Coverage-dependent faceting of Au chains on Si(557)

I. Barke,[1,2] F. Zheng,[2] S. Bockenhauer,[2] K. Sell,[1] V. v. Oeynhausen,[1] K. H. Meiwes-Broer,[1]
S. C. Erwin,[3] and F. J. Himpsel[2]
[1]*Institut für Physik, Universität Rostock, Universitätsplatz 3, D-18051 Rostock, Germany*
[2]*Department of Physics, University of Wisconsin Madison, 1150 University Avenue Madison, Wisconsin 53706, USA*
[3]*Center for Computational Materials Science, Naval Research Laboratory, Washington, DC 20375, USA*
(Received 18 December 2008; revised manuscript received 10 March 2009; published 1 April 2009)

The structural and electronic phase diagrams of Au on Si(557) are established using scanning tunneling microscopy (STM) and angle-resolved photoemission. Five phases consisting of altogether seven facets are observed in the submonolayer regime. With increasing Au coverage one observes Si(111)7×7+Si(112), Si(557)-Au, Si(111)5×2-Au+Si(335)-Au, Si(111)$\sqrt{3}\times\sqrt{3}$-Au+Si(335)-Au, and Si(111)$\sqrt{3}\times\sqrt{3}$-Au +Si(5 5 11)-Au. The relative surface areas of the five phases and seven facets are determined accurately by depositing a Au wedge ranging from 0 to 0.7 monolayer and performing automatic pattern recognition on large-scale STM images. Angle-resolved photoemission spectra are decomposed into contributions from the five phases. The Fermi wave vectors and the band filling of various facets are identified. Using Si(557)-Au as reference we find a coverage of three Au chains per unit cell for the frequently studied Si(111)5×2-Au surface (instead of the widely used value of two Au chains). Likewise a coverage of two Au chains per unit cell is found for Si(553)-Au (instead of one Au chain), in agreement with x-ray diffraction. A structural model with three Au rows per unit cell is developed for Si(111)5×2-Au using density-functional-theory calculations.

DOI: 10.1103/PhysRevB.79.155301 PACS number(s): 73.20.At, 79.60.Jv, 68.37.Ef, 68.47.Fg

I. MOTIVATION AND OUTLINE

Many metals lead to the formation of atomic chains on vicinal Si(111) surfaces at submonolayer coverage (for an overview see Refs. 1–6). Even the flat Si(111) surface frequently forms chain structures despite the fact that the chains break the threefold symmetry of the surface. It is quite likely that these surfaces are driven one-dimensional by the formation of the honeycomb chain,[7–13] a ribbon of connected Si hexagons. The honeycomb chain can be compared to a graphene ribbon[14] but made of silicon. It represents the narrowest possible ribbon but can be hundreds of nanometers long because it is perfectly lattice matched to the Si substrate along the $[1\bar{1}0]$ azimuth. In the perpendicular $[\bar{1}\bar{1}2]$ azimuth there is no lattice match at all, which causes the extremely narrow width of the honeycomb chain. Even though silicon does not form π-bonds in the bulk, it frequently does so at the surface where π-bonding becomes an important mechanism to heal broken bonds.

Metal-induced chain structures have created a versatile class of low-dimensional structures whose dimensionality can be varied between one and two by varying the terrace width.[12] A variety of unusual phenomena has been observed apart from the graphitic silicon ribbons. These include metallic chains of Au atoms connected by broken Si backbonds,[8–13,15] a mysterious band splitting[16–18] that was eventually revealed to be of magnetic origin,[9,19] fractional band filling,[18,20] nanoscale phase separation into metallic and semiconducting chain segments,[21–24] and charge-density waves.[25,26]

Metallic chains are particularly interesting because they may be viewed as the atomic limit of nanowires. In a Au chain on vicinal Si(111), for example, the overlap between the Au 6*s* orbitals and the Si sp^3 orbitals creates a chain of orbitals along which electrons can propagate. Metallic Au chain structures have been found on many vicinal Si(111) surfaces with odd Miller indices.[1–3,12] Obtaining high quality Au chain structures requires two parameters to be precisely adjusted, the surface orientation and the Au coverage. Therefore we have set out to investigate the phase diagrams of vicinal Si(111) surfaces versus Au coverage. As the Au coverage increases, combinations of several well-defined facets with well-defined orientations and Au coverages are formed. Well below a monolayer (ML) coverage these facets exhibit one-dimensional chain structures, and approaching a monolayer the two-dimensional Si(111)$\sqrt{3}\times\sqrt{3}$-Au structure starts to dominate the surface. Variants of the Si(111)$\sqrt{3}\times\sqrt{3}$-Au structure have been identified at higher coverages.[27,28] These will not be considered here since we are only interested in the low-coverage regime where the $\alpha\sqrt{3}\times\sqrt{3}$ variant dominates. It is interesting to note that Si and Au are not miscible in bulk, i.e., none of these surface alloys has a bulk counterpart.

We focus on the surface structures formed by Au on Si(557) with increasing Au coverage. A well-defined Si(557)-Au structure exists at a coverage of a single Au chain per unit cell. This structure will be used as reference for the Au coverage. It is by far the best-characterized of all the Au chain structures on vicinal silicon and the only one where first-principles band calculations match the angle-resolved photoemission data.

The Si(557)-Au structure was discovered quite early by electron diffraction[29] and has been investigated extensively in recent years. Scanning tunneling microscopy (STM) showed two atomic chains, one of them corresponding to a row of Si adatoms with doubled periodicity along the chains and the other corresponding to the honeycomb chain at the step edge.[17,26,30] The second-order low-energy electron diffraction (LEED) spots were found to be rather weak and spread into long streaks due to the lack of phase coherence

 ©2009 The American Physical Society

between adjacent adatom rows. The atomic structure was obtained from both x-ray diffraction[15] and total-energy minimization.[8,9,12,31] Angle-resolved photoemission revealed a split one-dimensional band.[16–19] A relativistic first-principles density-functional calculation gave a good description of the electronic structure seen in angle-resolved photoemission and explains the splitting to be of magnetic origin (due to spin-orbit interaction near the Au-chain atoms).[9] This prediction was confirmed by a high-resolution photoemission experiment which resolved the pattern of avoided band crossings on the related Si(553)-Au surface.[19] It was only compatible with a spin-orbit splitting (Rashba effect) and not with ferromagnetic, antiferromagnetic, or nonmagnetic bonding/antibonding splittings.

By combining STM and angle-resolved photoemission we are able to determine both the structural and the electronic phase diagram of the Si(557) surface versus Au coverage. The results provide a detailed experimental picture of several faceting transitions versus Au coverage which has direct implications on the analysis of integrating and averaging experimental methods. Faceting of Si has been a topic of long-term interest, both for clean[32] and metal-covered[4,33–37] surfaces. Our detailed results on the various facets and their electronic structure can serve as input for theoretical models of faceting at surfaces in general. A "wedge" technique is used where the Au coverage is varied from zero to almost one monolayer along the sample surface. The Au coverage of each facet structure is determined by a precise self-calibrating method which is based on the area ratio of different facets in large-area STM images. The electronic structure of these faceted phases is obtained by decomposing angle-resolved photoemission data from many points along a wedge into a linear combination of spectra from the five distinct phases. This allows us to obtain accurate Fermi wave vectors and band fillings.

From large-scale STM images we obtain an accurate coverage of 3.1 ± 0.2 Au chains per unit cell for the Si(111)5×2-Au surface. This differs from our previous estimate of two Au chains per unit cell and greatly narrows the range of other published coverage estimates of 2–4 chains per unit cell.[12,27,28,33,35,37–45] A similar analysis for the Si(553)-Au surface yields a coverage of 2.1 ± 0.4 chains per unit cell, which is again higher than previously estimated but consistent with the coverage of two Au chains per unit cell obtained from x-ray diffraction.[46]

In light of this coverage determination, most of the published structural models for Si(553)-Au and Si(111) 5×2-Au will require revision to accommodate an additional gold chain. No such revision is needed for Si(557)-Au; this might explain why the overall agreement between theory and experiment is better for Si(557)-Au[8,9] than for Si(553)-Au and Si(111)-5×2-Au.[10,11,13,47–51] In Sec. VII of this paper we propose a revised tentative structural model for Si(111)5×2-Au consistent with our coverage determination. We will present a more complete model in a future publication.[52]

II. EXPERIMENTAL TECHNIQUES

Si wafers (from Virginia Semiconductors) were degassed for several hours at 700 °C before flashing at 1250 °C for a few seconds. A rapid cool-down to 850 °C was followed by slow cooling to room temperature. An important prerequisite for obtaining well-defined chain structures was a flexible mount of the samples that prevented strain from building up during high-temperature flashing. Gold was evaporated from a Mo wire basket or from an electron-beam evaporator. We ensured that the adsorption coefficient was constant (approaching unity) by varying the sample temperature during evaporation over several 100 °C. The pressure was kept below 5×10^{-10} mbar throughout the sample preparation.

All STM measurements were carried out at room temperature with low tunneling currents (<50 pA). Photoelectron spectra were recorded at the PGM beamline of the Synchrotron Radiation Center (SRC) in Madison. The end station was equipped with a Scienta 200U electron analyzer and fully computer-controlled manipulator motion. The energy resolution was kept better than 20 meV and the angular resolution better than 0.2°.

For a detailed study of the coverage dependence an absolute calibration of the evaporator is crucial. The importance of hitting the correct coverage for Si(557)-Au was emphasized already in the initial photoemission work.[16] Microbalances based on a quartz crystal are typically used for this purpose but they suffer from a number of drawbacks. The temporal stability of the evaporation flux is usually limited, which makes simultaneous evaporation and thickness monitoring necessary. For submonolayer coverage it is difficult to achieve sufficient accuracy because of the heat load during the evaporation process.

Here we follow a different approach by using a structure with known Au coverage as a reference, i.e., Si(557)-Au. This structure contains one Au chain per unit cell. That corresponds to a coverage $\Theta_{557}=0.176$ ML, with 1 ML defined as the density of a Si atom layer on the Si(111) surface.

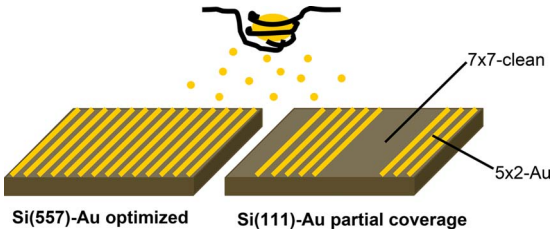

FIG. 1. (Color online) Method for the coverage determination of Au chain structures on vicinal and flat Si(111). The Si(557)-Au structure with one Au chain per unit cell is used as reference. The same amount of Au is deposited on other surfaces, such as Si(111)5×2-Au and Si(553)-Au. The relative areas of clean and Au-covered silicon uniquely determine the Au coverage.

III. ACCURATE COVERAGE DETERMINATION

Our method of determining accurate coverages is illustrated in Fig. 1: two silicon samples with different crystal orientations, in this case Si(557) and Si(111), are mounted on a sample holder next to each other. Au is deposited on both samples simultaneously, which assures the same coverage. The coverage is optimized by adjusting the evaporation time until the ideal Si(557)-Au structure is observed. This can be

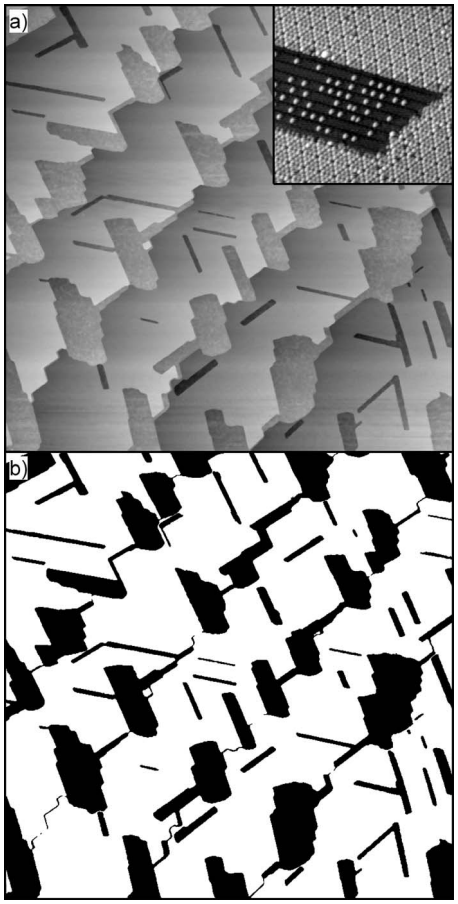

FIG. 2. Determination of the Au coverage for Si(111)5×2-Au: (a) STM images of the Si(111) surface (1×1 μm^2) after evaporation of the Au amount needed for the ideal Si(557)-Au surface [compare Fig. 3(a)]. Since the Au coverage for Si(111)5×2-Au is higher than for Si(557)-Au there is a coexistence of the clean Si(111)7×7 (light areas) and Si(111)5×2-Au (dark areas). The inset shows a close-up of the two structures (30×30 nm^2). (b) The Au covered part (black) has been extracted using an edge detection algorithm and subsequent flood filling.

judged very accurately by starting with low coverages and gradually eliminating the remaining stripes of clean Si(111)7×7 (compare Fig. 3 in Ref. 1 which clearly detects 2/100 of a monolayer undercoverage). On Si(111) the same amount of Au forms patches of Si(111)5×2-Au along with remaining clean Si(111)7×7 regions [Fig. 2(a)]. This is due to the higher Au coverage required for ideal Si(111)5×2-Au compared to Si(557)-Au. The Si(557)-Au and Si(111)5×2-Au facets exhibit chain structures with extra atoms on top of the chains. These are Si atoms, as demonstrated in Ref. 53. Therefore, they do not affect the Au coverage.

The accurate fraction b of Si(111)5×2-Au patches is determined by a semiautomated image processing method that recognizes different surface reconstructions [Fig. 2(b)]. The result is $b=0.283\pm0.020$. The residual error is dominated by the edges of the patches and their finite number within a STM frame. Taking the angle $\alpha=9.45°$ between the (557) and (111) into account results in a Au coverage of $\Theta_{5\times2}=\Theta_{557}\frac{\cos(\alpha)}{b}=(0.615\pm0.040)\mathrm{ML}=3.1\pm0.2$ Au chains per 5×2 unit cell. This result was reproduced by five large scale (≈1 μm^2) STM images obtained in three different evaporation experiments, all yielding values in the range of $\Theta_{5\times2}=0.57-0.65$ ML.

Our coverage result for Si(111)5×2-Au can be compared to many previous findings (see Refs. 12, 27, 28, 33, 35, and 38–45 and references therein). The value of 0.615 ± 0.040 ML is consistent with an accurate determination of the coverage ratio of 0.665 ± 0.010 ML between Si(111)5×2-Au and Si(111)$\alpha\sqrt{3}\times\sqrt{3}$-Au,[28,38] as long as a coverage of one monolayer is assumed for Si(111)$\alpha\sqrt{3}\times\sqrt{3}$-Au (compare the LEED analysis in Ref. 54 and a similar assumption in Ref. 33). The widely used coverage of two Au chains for Si(111)5×2-Au can be traced to the initial assumption of 2/3 monolayer coverage for Si(111)$\sqrt{3}\times\sqrt{3}$-Au,[28,38] which was kept implicitly in most subsequent work.

From the step movement during the growth of the Si(111)5×2-Au structure it was determined[45] that the Si atom density in the top double layer is 40% smaller than for clean unreconstructed Si(111). That is consistent with the larger number of Si atoms displaced by three Au chains instead of two. Indeed, the range of Au coverages determined in Ref. 45 straddles three Au chains (0.5–0.75 monolayer, i.e., 2.5–3.8 Au chains per unit cell).

IV. COVERAGE-DEPENDENT FACETING FROM STM

The Si(557)-Au surface begins to facet when going away from the optimum Au coverage. This happens both toward lower and higher coverages. The clean Si(557) surface consists of two facets, i.e., Si(111)7×7 and Si(112).[55–57] When adding Au one obtains three facets, i.e., a Si(557)-Au facet in addition to the two clean facets. For coverages higher than one Au chain per unit cell we observe a sequence of three more well-defined phases, each consisting of a distinct combination of two facets at a particular Au coverage. In between these pure phases we have phase mixtures with more than two facets. The relative areas of the observed facets are constrained by two conditions that must be fulfilled at any Au coverage:

(1) The average slope of the surface must match the sample miscut of 9.45° for Si(557).

(2) The *average* Au coverage [corrected for the projection onto the (557) plane] must correspond to the amount of deposited Au.

Since the area ratio between two facets in a phase is constant by definition, the area ratio between two coexisting phases is uniquely determined by the Au coverage. A combination of STM and angle-resolved photoemission allows us to quantitatively follow the evolution of the surface as a function of Au coverage. In the following we first identify the phases by STM (Fig. 3) and then investigate their electronic structure by angle-resolved photoemission.

The clean Si(557) surface (phase 1) has been found to consist of alternating facets of (111) and (112) orientation, respectively.[55–57] The (111) facet is one 7×7 unit-cell wide. Upon deposition of one Au chain per unit cell the surface transforms to phase 2, the one-dimensional Si(557)-Au struc-

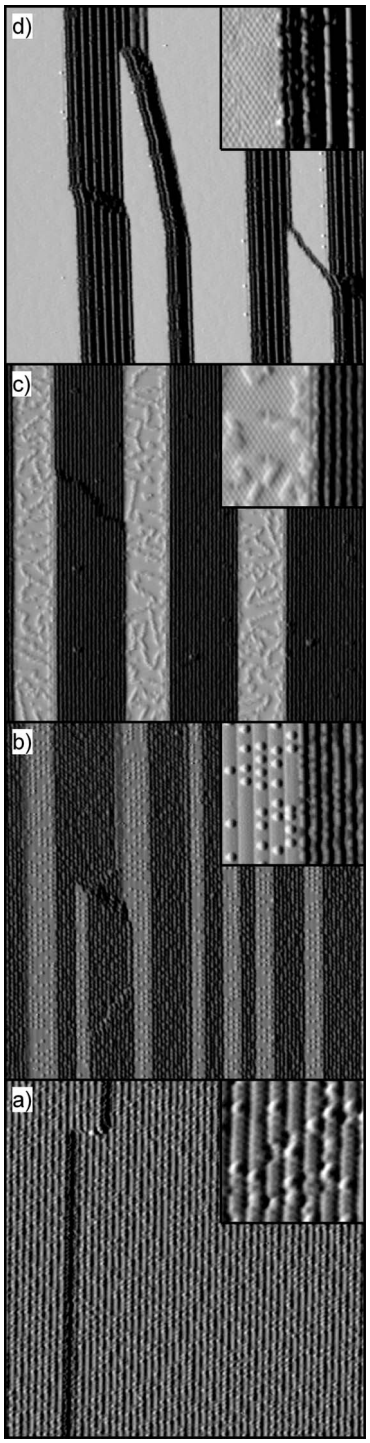

FIG. 3. STM images of the Si(557)-Au surface at various Au coverages (increasing from bottom to top). Different facets appear in different shades of gray, since the derivative of the height is shown, i.e., the slope of a facet. Thereby the surface appears to be illuminated from the left, casting shadows to the right (in the $[\bar{1}\bar{1}2]$ direction). (a) The Si(557)-Au phase (phase 2) at a coverage $\Theta = 0.176$ ML [in units of Si(111) monolayers]. (b) Coexistence of Si(111)5×2-Au and Si(335)-Au facets at $\Theta \approx 0.39$ ML (phase 3). (c) Coexistence of Si(111)$\sqrt{3}\times\sqrt{3}$-Au and Si(335)-Au facets at $\Theta \approx 0.53$ ML (phase 4). (d) Coexistence of Si(111)$\sqrt{3}\times\sqrt{3}$-Au and Si(5 5 11)-Au facets at $\Theta \approx 0.64$ ML (phase 5). Image size: 100×100 nm^2 (insets 15×15 nm^2).

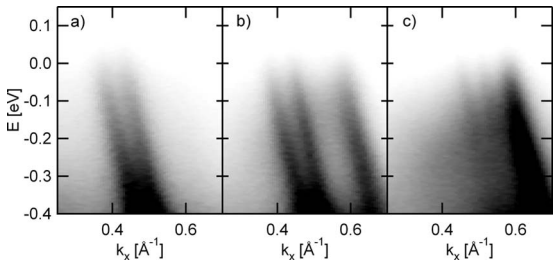

FIG. 4. Angle-resolved photoemission from Au-induced chain structures on Si(557), showing the band dispersion in the direction of the Au chains. High photoemission intensity is shown dark. The photon energy is 44 eV. (a) Si(557)-Au (phase 2). (b) Coexistence of Si(557)-Au, Si(111)5×2-Au, and Si(335)-Au (phase 2 plus phase 3). (c) Coexistence of Si(111)5×2-Au and Si(335)-Au (phase 3).

ture with an optimum Au coverage $\Theta_2 = 0.18$ ML [Fig. 3(a)]. STM images of three more phases at higher Au coverages are shown in Figs. 3(b)–3(d). At $\Theta_3 = 0.39$ ML phase 3 is reached, consisting of Si(111)5×2-Au and Si(335)-Au facets. Further increase in the Au coverage transforms the Si(111)5×2-Au facets into Si(111)$\sqrt{3}\times\sqrt{3}$-Au facets with $\Theta_4 = 0.53$ ML, while the Si(335)-Au facets remain (phase 4). Eventually the Si(335)-Au facets make room for Si(5 5 11)-Au facets at a coverage $\Theta_5 = 0.64$ ML (phase 5). It is important to note that these Si(5 5 11)-Au facets differ from those observed on a Si(5 5 12) surface.[34,58] The Au content is significantly lower in our case, and the interchain distance is larger (see the photoemission section below). It is likely that the nearby Si(111)$\sqrt{3}\times\sqrt{3}$-Au facets act as Au sinks. The resulting shift of the chemical potential might stabilize a structure which would not be stable by itself.

Overall, we find seven different facets in five different phases. All structures are stable against annealing up to 900 °C and their relative area fraction is independent of the annealing temperature. Only the overall size of the facets increases with high-temperature annealing.

Our results explain the previous observation[16] that the half-order streaks in the LEED pattern need to be minimized for obtaining optimal angle-resolved photoemission patterns from Si(557)-Au. These streaks become stronger when Si(111)5×2-Au facets are starting to form at excess Au coverage.

At higher coverages $\Theta > \Theta_5$ the Si(111)$\sqrt{3}\times\sqrt{3}$-Au facets keep growing and Si(5 5 11)-Au is replaced by increasingly steeper facets that are not analyzed in detail in this work.

V. ELECTRONIC PHASE DIAGRAM FROM ANGLE-RESOLVED PHOTOEMISSION

While STM detects different facets of a phase directly, photoemission averages over macroscopic sample areas. Therefore, the resulting spectra represent a weighted combination of all facets. The dispersion of the relevant bands near the Fermi level is obtained from angle-resolved photoemission with energy and angular multidetection. The resulting photoemission intensity versus energy and momentum is shown in Fig. 4 for three different Au coverages. High pho-

toemission intensity is shown dark for better clarity. The three panels correspond to a transition from Si(557)-Au (phase 2) to Si(111)5×2-Au+Si(335)-Au (phase 3) with a phase mixture in between. At $\Theta_2=0.18$ ML the surface is entirely covered by Si(557)-Au which exhibits a spin-split doublet of half-filled bands [Fig. 4(a)].[9,19] Further deposition of Au results in a new energy band [Fig. 4(b)] which originates from facets of Si(111)5×2-Au that are part of the phase 3 [see Fig. 3(b)].[21,23] This band reaches its maximum intensity at $\Theta_3=0.39$ ML. Also, the Si(557)-Au doublet disappears and a new doublet appears which exhibits slightly lower electron filling [Fig. 4(c)]. These are the spin-split bands of the Si(335)-Au facet which can be identified by their Fermi wave vector.[12]

In order to study the coverage dependence systematically we now focus on the Fermi level crossings which provide the one-dimensional Fermi wave vectors. The Au coverage is varied continuously by creating a wedge-shaped coverage profile $\Theta(z)$ across the Si sample. A simple translation of the sample along z scans through the whole coverage regime (typically from 0 to ≤ 1 monolayer). The profile of the synchrotron beam has a width $\delta z \approx 0.1$ mm in the direction of the coverage gradient. Together with a total sample length $\Delta z > 10$ mm the entire relevant coverage range can be investigated with a resolution of up to 0.01 monolayer, all with the same Au deposition. A linear coverage profile is obtained by moving the sample behind a knife edge during Au evaporation with stepping motor control and electronic position readout. The coverage profile is confirmed by monitoring the Au 5*d* electron intensity [see Fig. 6(d)].

Momentum distribution curves (MDCs) are shown in Fig. 5 for Au coverages from zero up to $\Theta \approx 0.7$ ML. Various peaks appear as a function of Au coverage which can be assigned to the Fermi wave vectors of specific facets. Features *A*, *C*, and *D* correspond to the spin-split bands of Si(557)-Au, Si(335)-Au,[12] and Si(5 5 11)-Au, respectively. The strong peak *B* stems from Si(111)5×2-Au regions. Although there are three different chain structures giving rise to spin-split bands (features *A*, *C*, and *D*) they can be clearly distinguished by their Fermi wave vectors. All one-dimensional chain structures exhibit steep bands close to the Fermi level that result in sharp peaks in Fig. 5. However, the two-dimensional Si(111)7×7 and Si(111)$\sqrt{3}\times\sqrt{3}$-Au structures do not have such steep metallic bands in the narrow k range investigated here, giving rise to smooth but characteristic momentum distributions.

The average Au coverage Θ_{av} of a particular phase can be decomposed into the contributions from two coexisting facets via $\Theta_{av}=\frac{A_1^{rel}}{\cos\alpha_1}\Theta_1+\frac{A_2^{rel}}{\cos\alpha_2}\Theta_2$, where $\Theta_{1,2}$ are the optimum Au coverages of facets 1 and 2, $\alpha_{1,2}$ are the positive angles of the two facets relative to (557), and $A_{1,2}^{rel}$ are the fractional areas with respect to the (557) orientation obtained from $A_{1,2}^{rel}=(1+\tan\alpha_{1,2}/\tan\alpha_{2,1})^{-1}$. The new Au coverage $\Theta=0.6$ ML for Si(111)5×2-Au and available models for the other structures[12,59] result in the values listed in Table I.

The evolution of the spectral features with Au coverage is quantified by decomposing the MDCs into contributions from the five phases. We do not attempt to decompose the MDC further into facets but extract the Fermi wave vectors of the facets (see Table II). For the decomposition of the photoemission data we switch to a two-dimensional representation of the data as shown in Fig. 6(a). The coverage dependence (i.e., the z position on the sample) is plotted

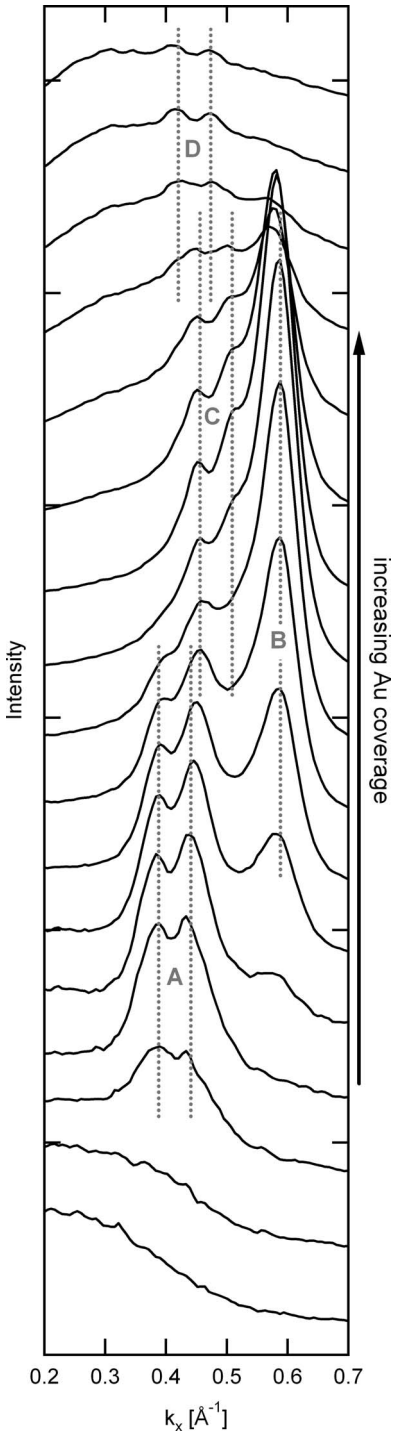

FIG. 5. Momentum distribution curves at E_F along the chain direction (horizontal cuts in Fig. 4). The Au coverage increases from bottom to top. The peaks *A*-*D* correspond to the Fermi wave vectors of the following facets (see Table II): (A) Si(557)-Au, (B) Si(111)5×2-Au, (C) Si(335)-Au, and (D) Si(5 5 11)-Au. The splitting of *A*, *C*, and *D* is due to the spin-orbit interaction (Refs. 9 and 19).

TABLE I. Overview of the various phases observed on Si(557). Each phase consists of one or two structures as indicated in the second and third column. Subsequent columns contain the angles $\alpha_{1,2}$ of the facets with respect to the (557) direction, the relative area fractions $A_{1,2}^{\mathrm{rel}}$, and the optimum Au coverages $\Theta_{1,2}$ of the respective structures. In the last column the average Au coverage Θ_{av} for each phase is given.

Phase	Facet structure 1	Facet structure 2	α_1 (°)	α_2 (°)	A_1^{rel}	A_2^{rel}	Θ_1 (ML)	Θ_2 (ML)	Θ_{av} (ML)
1	Si(111)7×7	Si(112)	9.45	19.5	0.52	0.48	0	0	0
2	Si(557)-Au		0		1		0.18		0.18
3	Si(111)5×2-Au	Si(335)-Au	9.45	4.97	0.34	0.66	0.6	0.27	0.39
4	Si(111)$\sqrt{3}\times\sqrt{3}$-Au	Si(335)-Au	9.45	4.97	0.34	0.66	1.0	0.27	0.53
5	Si(111)$\sqrt{3}\times\sqrt{3}$-Au	Si(5 5 11)-Au	9.45	12.6	0.57	0.43	1.0	0.14	0.64

along the x axis and the momentum along the y axis. Dark features correspond to Fermi wave vectors versus coverage. As a first approximation for the momentum distributions of the five phases we use vertical cuts at the dashed lines in Fig. 6(a) where the characteristic features of five phases dominate. The MDC for clean Si(111)7×7 is taken at the z position for the onset of the Au wedge, as determined from the Au 5d signal in Fig. 6(d). For the other four MDC the z positions that correspond to the coverages as listed in Table I are used. These MDC form a set of five basis spectra $b_i(k_x)$ $(i=1\ldots5)$ which are used to approximate the measured MDC $d_j(k_x)$ at any Au coverage $\Theta_j=\Theta(z_j)$ by a linear combination. The index j lists the z positions along the wedge. The MDC are approximated by the linear combinations $f_j(k_x)=\Sigma_i c_{ij} b_i(k_x)$. Their deviation from the data $[f_j(k_x)-d_j(k_x)]^2$ is minimized with respect to the coefficients $c_{ij}=c_i(z_j)$ by a least-squares fit with the constraints $0\leq c_{ij}\leq 1$. The outcome of the fit is a set of five coefficients $c_i(z)$, such as those shown in Fig. 6(c). However, there is still a remaining scaling parameter that couples the measured Au 5d intensity to the Au coverage on the sample. This parameter is optimized by the same least-square fit as the other parameters. The resulting fit to the experimental MDC is shown in Fig. 6(b), and the corresponding coefficients $c_i(z)$ of the five phases are plotted in Fig. 6(c). There is good agreement between Figs. 6(a) and 6(b) and each $c_i(z)$ exhibits only a single sharp maximum with nearly linear sections in between, thus providing further confidence of this data analysis.

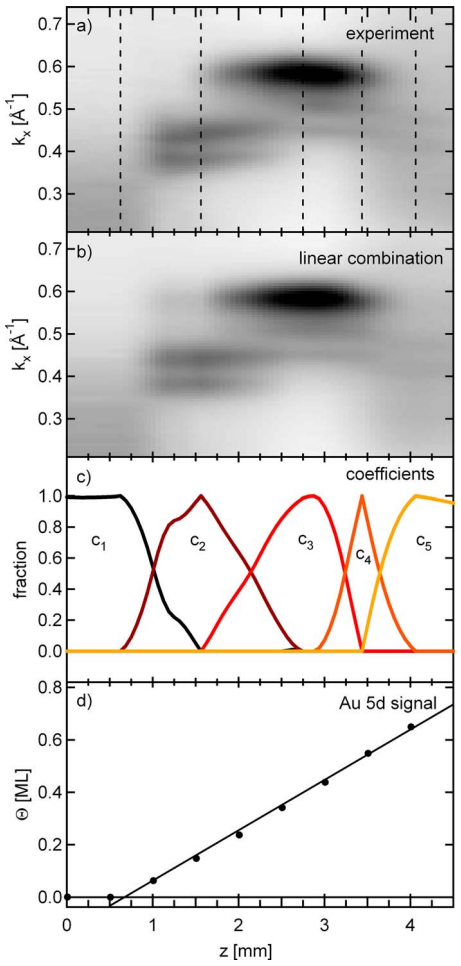

FIG. 6. (Color online) Momentum distribution (vertical) versus Au coverage (horizontal), measured using a Au wedge ranging from 0.0 to 0.7 monolayer. High photoelectron intensity is shown dark. (a) Experimental data. (b) Best fit of (a) using linear combinations of momentum distributions from the five observed phases [vertical dashed lines in (a)]. (c) Normalized coefficients for the fit in (b). Each coefficient is the fraction of the surface covered by the corresponding phase. (d) The integrated Au 5d photoemission intensity, confirming the linear increase in the Au coverage along the Au wedge.

The little shoulder of $c_2(z)$ at $z=1.2$ mm in Fig. 6(c) is due to a photovoltage shift of the spectra in this coverage region caused by a strong initial change in the Fermi-level pinning with Au deposition which is difficult to correct. This

TABLE II. Comparison of Fermi wave vectors of the four chain structures observed on Si(557). Three of these structures exhibit spin-split bands distinguished by $\Delta k_{F,1}$ and $\Delta k_{F,2}$. Δk_F is the difference from the average of the two Fermi wave vectors measured for Si(557)-Au, which is approximately half the Brillouin-zone boundary (0.41 Å^{-1}).

Chain structure	$\Delta k_{F,1}$ (Å^{-1})	$\Delta k_{F,2}$ (Å^{-1})
Si(557)-Au	−0.025	0.025
Si(335)-Au	0.035	0.095
Si(111)5×2-Au	0.175[a]	
Si(5 5 11)-Au	0.005	0.055

[a]This band is different from the spin-orbit-split bands listed for the other surfaces. It contains both spins.

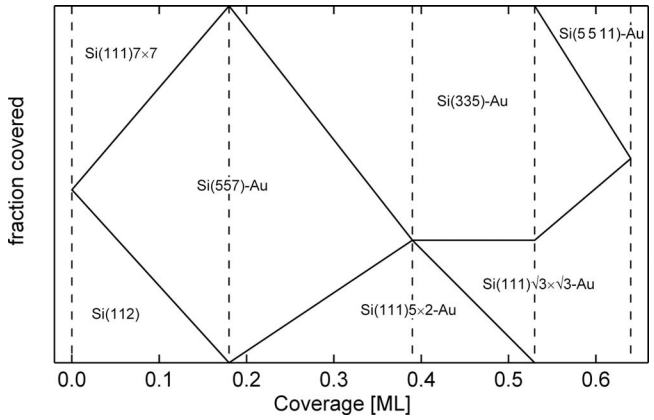

FIG. 7. Phase diagram of Au on Si(557) versus Au coverage. The five observed phases are indicated by vertical dashed lines [the same as in Fig. 6(a)]: phase 1: Si(111)7×7+Si(112); phase 2: Si(557)-Au; phase 3: Si(111)5×2-Au+Si(335)-Au; phase 4: Si(111)$\sqrt{3}\times\sqrt{3}$-Au+Si(335)-Au; phase 5: Si(111)$\sqrt{3}\times\sqrt{3}$-Au +Si(5 5 11)-Au. The full lines delineate the fractional areas of the seven different facets that make up the five phases.

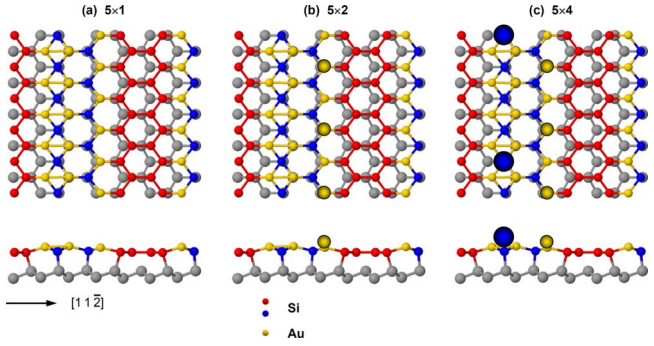

FIG. 8. (Color online) Tentative proposed structural model of Si(111)5×2-Au consistent with the new coverage determination of three Au rows per unit cell (instead of two). (a) A 5×1 model suggested by total-energy calculations. (b) A 5×2 schematic variant with buckling along one of the gold chains. Although this buckling is suggested by STM images of the undoped regions, it is not stable in total-energy calculations. (c) A 5×4 model with Si adatoms (largest circles) as found experimentally in the doped regions. A comprehensive theoretical study will be published separately (Ref. 52).

energy shift causes a shift of the Fermi wave vector due to the band dispersion. It can be seen in Fig. 6(a) as an upward shift of the split Fermi surface with increasing coverage.

The five c_i correspond to the relative abundance of the five phases and thus are related to the Au coverage if the coverage of the facets is known. Calculated coverages according to available facet models are listed in Table I. This quantitative analysis of the photoemission data provides independent corroboration of the conclusion obtained from the STM data in Sec. III that the Si(111)5×2-Au surface has three Au chains per unit cell, not two. Assuming two Au chains would place the maximum contribution of the Si(111)5×2-Au MDC (third dashed line) at the position z =2.25 mm, which is far away from the maximum intensity of the strong band B (Fig. 5) that is a feature of Si(111)5 ×2-Au. Furthermore, the optimized linear combination does not fit the data anymore and results in a six times larger deviation (not shown).

Figure 7 summarizes the evolution of the five phases and seven facets with increasing Au coverage. Solid lines delineate the fraction of the surface covered by specific facets. The five pure phases appear at the intersections of these lines where one facet vanishes and a new facet appears. The corresponding coverages are indicated by dashed vertical lines. At Θ=0.3 ML, for instance, the surface consists of a combination of phase 2 (Si(557)-Au) and phase 3 [Si(111)5 ×2-Au+Si(335)-Au]. About 43% of the area is covered by Si(557)-Au, 20% by Si(111)5×2-Au and the remaining 37% by Si(335)-Au.

The coexistence of several chain structures on a single sample provides the opportunity to compare their Fermi-level crossings with high accuracy. Table II lists the Fermi wave vectors k_F for Si(557)-Au, Si(335)-Au, Si(111)5 ×2-Au, and Si(5 5 11)-Au. The Si(557)-Au surface serves as a reference for the Fermi wave-vector differences Δk_F listed in Table II. These differences are taken from the average of the two spin-split Fermi wave vectors of Si(557)-Au, which is approximately half the Brillouin-zone boundary (0.41[Å^{-1}], see Refs. 12 and 26). This splitting is observed for all chain structures except Si(111)5×2-Au (see Fig. 5). The band filling increases as the Fermi wave vector decreases because the band minima lie near the boundary of the one-dimensional Brillouin zone. Both spin-split bands have identical filling since they are shifted in k for a Rashba-type spin splitting, not in E.

VI. IMPLICATIONS FOR STRUCTURAL MODELS

We have pursued theoretically the implications of our coverage results for structural models. Extensive theoretical studies have been performed in the past for Si(111)5 ×2-Au under the assumption of two Au rows per unit cell.[10,11,13,47,48] We have investigated a variety of models having, instead, three Au rows. From total-energy calculations within density-functional theory we have identified two closely related 5×1 structures with very low surface energy. One of them, shown in Fig. 8(a), is reasonably consistent with spectroscopic STM images[52] when Si adatoms are included as shown in Fig. 8(c). The other structure (not shown here) is a mirror image of Fig. 8(a) constructed by reflecting the entire top layer of Si and Au atoms through a plane normal to the surface and parallel to the chains (or, equivalently, by simply shifting the central row of Au atoms in Fig. 8 toward the upper right, to the next triangular lattice site). This mirror configuration is also consistent with STM images.[13,24,52]

The 5×1 structure shown in Fig. 8(a) is only an approximate description of the real surface, which separates into short chain sections with a 5×2 reconstruction [Fig. 8(b)] and into 5×4 sections with Si adatoms on top of the 5×2 chains [Fig. 8(c)].[10,21,22,53,60] Density-functional investigations of these higher-order periodicities are still in progress.[52] The location of the Si adatoms in the 5×4 structure relative

to the buckled chains can be inferred from STM images. Schematic models of the two sections are shown in Figs. 8(b) and 8(c). A complete model of the Si(111)5×2-Au surface would then consist of alternating adatom-free 5×2 regions and adatom-decorated 5×4 regions.[21–23,60] Each of these regions covers half of the surface. The adatoms may act as charge dopants and lead to charge transfer between the two regions.[10,22] A band-structure calculation of the complete Si(111)5×2-Au surface can be tested against angle-resolved photoemission data of the equilibrium structure[21] and their decomposition into contributions from undoped and doped regions.[23] A more comprehensive theoretical investigation of these issues will be published shortly.[52]

VII. CONCLUSIONS

In summary, we combine scanning tunneling microscopy and angle-resolved photoemission to determine both the structural and electronic phase diagrams of Au on Si(557)-Au, a vicinal Si(111) surface. Submonolayer Au wedges are used for a quantitative decomposition of the STM images and the photoemission spectra into contributions from different surface phases. For Au on Si(557) we find a remarkably complex phase diagram that is driven by the disproportionation of the surface into Au-rich and Au-depleted facets. As the coverage increases, the facet structures change from one-dimensional Au chains to a two-dimensional gold layer. By contrast, Au exhibits a very simple phase diagram on Si(553) which is similar to Si(557), except for interchanging the uphill and downhill directions. For Si(553) we find only a single phase with two Au rows per unit cell. Furthermore, the widely used coverage value of two Au rows for Si(111)5×2-Au needs to be revised to three Au rows. As a first step, we propose a tentative structural model for Si(111)5×2-Au based on density-functional-theory calculations and spectroscopic STM images.

ACKNOWLEDGMENTS

This work was supported by the NSF under Awards No. DMR-0705145 and No. DMR-0084402 (SRC) and by the DFG within the priority program No. SPP 1153, and by the Office of Naval Research. I.B. acknowledges support from the DAAD. Computations were performed at the DoD Major Shared Resource Center at AFRL.

[1] J. N. Crain and F. J. Himpsel, Appl. Phys. A: Mater. Sci. Process. **82**, 431 (2006).
[2] I. Barke, T. K. Rügheimer, F. Zheng, and F. J. Himpsel, Appl. Surf. Sci. **254**, 4 (2007).
[3] I. Barke, R. Bennewitz, J. N. Crain, S. C. Erwin, A. Kirakosian, J. L. McChesney, and F. J. Himpsel, Solid State Commun. **142**, 617 (2007).
[4] M. Czubanowski, A. Schuster, S. Akbari, H. Pfnür, and C. Tegenkamp, New J. Phys. **9**, 338 (2007).
[5] N. Oncel, J. Phys.: Condens. Matter **20**, 393001 (2008).
[6] I. Matsuda and S. Hasegawa, J. Phys.: Condens. Matter **19**, 355007 (2007).
[7] S. C. Erwin and H. H. Weitering, Phys. Rev. Lett. **81**, 2296 (1998).
[8] D. Sanchez-Portal, J. D. Gale, A. Garcia, and R. M. Martin, Phys. Rev. B **65**, 081401(R) (2002).
[9] D. Sanchez-Portal, S. Riikonen, and R. M. Martin, Phys. Rev. Lett. **93**, 146803 (2004).
[10] S. C. Erwin, Phys. Rev. Lett. **91**, 206101 (2003).
[11] S. Riikonen and D. Sanchez-Portal, Phys. Rev. B **71**, 235423 (2005).
[12] J. N. Crain, J. L. McChesney, F. Zheng, M. C. Gallagher, P. C. Snijders, M. Bissen, C. Gundelach, S. C. Erwin, and F. J. Himpsel, Phys. Rev. B **69**, 125401 (2004).
[13] H. S. Yoon, J. E. Lee, S. J. Park, I. W. Lyo, and M. H. Kang, Phys. Rev. B **72**, 155443 (2005).
[14] Y. W. Son, M. L. Cohen, and S. G. Louie, Phys. Rev. Lett. **97**, 216803 (2006).
[15] I. K. Robinson, P. A. Bennett, and F. J. Himpsel, Phys. Rev. Lett. **88**, 096104 (2002).
[16] P. Segovia, D. Purdie, M. Hengsberger, and Y. Baer, Nature (London) **402**, 504 (1999).
[17] R. Losio, K. N. Altmann, A. Kirakosian, J. L. Lin, D. Y. Petrovykh, and F. J. Himpsel, Phys. Rev. Lett. **86**, 4632 (2001).
[18] J. N. Crain, A. Kirakosian, K. N. Altmann, C. Bromberger, S. C. Erwin, J. L. McChesney, J. L. Lin, and F. J. Himpsel, Phys. Rev. Lett. **90**, 176805 (2003).
[19] I. Barke, F. Zheng, T. K. Rügheimer, and F. J. Himpsel, Phys. Rev. Lett. **97**, 226405 (2006).
[20] P. C. Snijders, S. Rogge, and H. H. Weitering, Phys. Rev. Lett. **96**, 076801 (2006).
[21] J. L. McChesney, J. N. Crain, V. Perez-Dieste, F. Zheng, M. C. Gallagher, M. Bissen, C. Gundelach, and F. J. Himpsel, Phys. Rev. B **70**, 195430 (2004).
[22] H. S. Yoon, S. J. Park, J. E. Lee, C. N. Whang, and I. W. Lyo, Phys. Rev. Lett. **92**, 096801 (2004).
[23] W. H. Choi, P. G. Kang, K. D. Ryang, and H. W. Yeom, Phys. Rev. Lett. **100**, 126801 (2008).
[24] E. Bussmann, S. Bockenhauer, F. J. Himpsel, and B. S. Swartzentruber, Phys. Rev. Lett. **101**, 266101 (2008).
[25] J. R. Ahn, P. G. Kang, K. D. Ryang, and H. W. Yeom, Phys. Rev. Lett. **95**, 196402 (2005).
[26] J. R. Ahn, H. W. Yeom, H. S. Yoon, and I. W. Lyo, Phys. Rev. Lett. **91**, 196403 (2003).
[27] T. Nagao, S. Hasegawa, K. Tsuchie, S. Ino, C. Voges, G. Klos, H. Pfnür, and M. Henzler, Phys. Rev. B **57**, 10100 (1998).
[28] W. Swiech, E. Bauer, and M. Mundschau, Surf. Sci. **253**, 283 (1991).
[29] M. Jalochowski, M. Strozak, and R. Zdyb, Surf. Sci. **375**, 203 (1997).
[30] M. Schöck, C. Sürgers, and H. v. Löhneysen, Europhys. Lett. **74**, 473 (2006).
[31] S. Riikonen and D. Sanchez-Portal, Phys. Rev. B **76**, 035410 (2007).

[32] E. D. Williams and N. C. Bartelt, Science **251**, 393 (1991).
[33] L. Seehofer, S. Huhs, G. Falkenberg, and R. L. Johnson, Surf. Sci. **329**, 157 (1995).
[34] A. A. Baski, K. M. Saoud, and K. M. Jones, Appl. Surf. Sci. **182**, 216 (2001).
[35] R. Hild, C. Seifert, M. Kammler, F. Heringdorf, M. Horn von Hoegen, R. A. Zhachuk, and B. Z. Olshanetsky, Surf. Sci. **512**, 117 (2002).
[36] H. Minoda, K. Yagi, F. J. Meyer zu Heringdorf, A. Meier, D. Kahler, and M. Horn von Hoegen, Phys. Rev. B **59**, 2363 (1999).
[37] J. D. O'Mahony, J. F. McGilp, C. F. J. Flipse, P. Weightman, and F. M. Leibsle, Phys. Rev. B **49**, 2527 (1994).
[38] E. Bauer, Surf. Sci. **250**, L379 (1991).
[39] L. E. Berman, B. W. Batterman, and J. M. Blakely, Phys. Rev. B **38**, 5397 (1988).
[40] C. Schamper, W. Moritz, H. Schulz, R. Feidenhansl, M. Nielsen, F. Grey, and R. L. Johnson, Phys. Rev. B **43**, 12130 (1991).
[41] L. D. Marks and R. Plass, Phys. Rev. Lett. **75**, 2172 (1995).
[42] K. N. Altmann, J. N. Crain, A. Kirakosian, J.-L. Lin, D. Y. Petrovykh, F. J. Himpsel, and R. Losio, Phys. Rev. B **64**, 035406 (2001).
[43] G. LeLay, Surf. Sci. **132**, 169 (1983).
[44] R. Plass and L. D. Marks, Surf. Sci. **380**, 497 (1997).
[45] Y. Tanishiro, K. Yagi, and K. Takayanagi, Surf. Sci. **234**, 37 (1990).
[46] S. K. Ghose, I. K. Robinson, P. A. Bennett, and F. J. Himpsel, Surf. Sci. **581**, 199 (2005). The model given here produces a band structure[50,61] that does not agree with photoemission. X-ray diffraction is dominated by Au, the high Z element, and much less sensitive to the positions of the Si atoms. That leaves many other models with the same Au rows, but different Si arrangements, to be considered.
[47] S. C. Erwin and C. Seifert, http://meetings.aps.org/link/BAPS.2006.MAR.R12.5
[48] F. C. Chuang, C. H. Hsu, C. Z. Wang, and K. M. Ho, Phys. Rev. B **77**, 153409 (2008).
[49] S. Riikonen and D. Sanchez-Portal, Nanotechnology **16**, S218 (2005).
[50] K. D. Ryang, P. G. Kang, H. W. Yeom, and S. Jeong, Phys. Rev. B **76**, 205325 (2007).
[51] S. Riikonen and D. Sanchez-Portal, Phys. Rev. B **77**, 165418 (2008) Despite the incorrect coverage used in this work, reasonable agreement with photoemission data was obtained.
[52] S. C. Erwin, I. Barke, and F. J. Himpsel (unpublished).
[53] R. Bennewitz, J. N. Crain, A. Kirakosian, J.-L. Lin, J. L. McChesney, D. Y. Petrovykh, and F. J. Himpsel, Nanotechnology **13**, 499 (2002).
[54] J. Quinn, F. Jona, and P. M. Marcus, Phys. Rev. B **46**, 7288 (1992).
[55] A. Kirakosian, R. Bennewitz, J. N. Crain, T. Fauster, J. L. Lin, D. Y. Petrovykh, and F. J. Himpsel, Appl. Phys. Lett. **79**, 1608 (2001).
[56] C. Tegenkamp, Z. Kallassy, H. Pfnür, H. L. Gunter, V. Zielasek, and M. Henzler, Phys. Rev. Lett. **95**, 176804 (2005).
[57] D. H. Oh, M. K. Kim, J. H. Nam, I. Song, C. Y. Park, S. H. Woo, H. N. Hwang, C. C. Hwang, and J. R. Ahn, Phys. Rev. B **77**, 155430 (2008).
[58] J. R. Ahn, H. W. Yeom, E. S. Cho, and C. Y. Park, Phys. Rev. B **69**, 233311 (2004).
[59] Since for the observed Si(5 5 11)-Au structure no model is available we assumed that the Au coverage corresponds to one Au row per unit cell, which is consistent with our photoemission data on the Au wedge.
[60] A. Kirakosian, R. Bennewitz, F. J. Himpsel, and L. W. Bruch, Phys. Rev. B **67**, 205412 (2003).
[61] S. Riikonen and D. Sanchez-Portal, Surf. Sci. **600**, 1201 (2006).